Geomechanics and Engineering, *Vol. 34, No. 6 (2023) 611-621*
https://doi.org/10.12989/gae.2023.34.6.611

Numerical investigation of effect of geotextile and pipe stiffness on buried pipe behavior

Candas Oner[1a], Selcuk Bildik*[2] and J. David Frost[1b]

[1]*School of Civil Engineering, Georgia Institute of Technology, 790 Atlantic Drive, Atlanta, GA, USA*
[2]*Department of Civil Engineering, Nisantasi University, Tasyoncasi Street No:1V-1Y, Maslak, Istanbul, Turkey*

(*Received June 12, 2022, Revised June 20, 2023, Accepted August 10, 2023*)

Abstract. This paper presents the results of a numerical investigation of the effect of geotextile reinforcement on underlying buried pipe behavior using PLAXIS 3D. In this study, variable parameters such as the in-plane stiffness of the geotextile, the pipe stiffness, the soil stiffness, the footing width, the geotextile width, and the location of the geotextile reinforcement layer are investigated. Deflections and bending moments acting on the pipe are evaluated for different combinations of variables and are presented graphically. It is observed that with an increase in the in-plane stiffness of the geotextile reinforcement, there is a tendency for a decrease in both deflections in the pipe and bending moments acting on the pipe. Conversely, with an increase in the pipe stiffness, geotextile reinforcement efficiency decreases. In the investigated region of soil stiffness, for the given pipe and geotextile stiffness, an optimum efficiency of geotextile is observed in medium dense soils. Further, it is shown that relative lengths of geotextile and footing has an important role on geotextile efficiency. Lastly, it is also demonstrated that relative location of geotextile layer with respect to the buried pipe plays an important role on the geotextile efficiency in reducing the bending moments acting on the pipe and deflections in the pipe. In general, geotextiles are more efficient in reducing the bending moments as opposed to reducing deflections of the pipe. Numerical validation is done with an experimental study from the literature to observe the applicability of the numerical model used.

Keywords: bending moment; buried pipes; deflection; finite element; geotextile

1. Introduction

Buried pipe systems are one of the most important civil engineering infrastructure components that involve soil-structure interaction. They carry significant importance in the transmission of water, gas, sewage, and many other systems. As buried structures, their interaction with the surrounding soil is of utmost importance in understanding their response. Accurate estimation of the vulnerability of the pipe to anticipated loads is thus essential in protecting the infrastructure system. In the case of possible leakage or failure of these systems, immediate actions need to be taken; however, this may not be an easy task as they are buried structures. In the literature, there are several studies reported to help understand soil-pipe interaction. These studies can be categorized as experimental, analytical, and numerical (Aria *et al*. 2017, 2019, Bildik and Laman 2015, 2019, 2020, Beju and Mandal 2017, Elshesheny *et al.* 2020, Hegde and Sitharam 2015, Fattah *et al.* 2018, Kou *et al.* 2018, Kou and Shukla 2019, 2021, Ma *et al*. 2019, Pires and Palmeria 2017, 2021, Placido and Portelinha 2019).

Geosynthetics, which are used for many functions in practice, have also been used for the reinforcement of buried structures. Bildik and Laman (2020) conducted physical model experiments to find out the effect of geogrid reinforcement on the bearing capacity, footing settlement, and hoop stresses on the pipe. They determined the optimum depth of the geogrid and an optimum number of geogrids. Pires and Palmeria (2017) investigated the effect of the geogrid orientation on the model footing settlement, pressures acting on the pipe, and strains in the pipe. They tested three different orientation types, including horizontal, inverted U shaped, and enveloped, which means that pipe is fully surrounded with the geogrid. Overall, inverted U and enveloped type configurations yielded better results in terms of reducing the vertical and horizontal stresses acting on the pipe compared to horizontal reinforcement. Ma *et al*. (2019) investigated the effect of thickness of overlying EPS Geofoam blocks on the pressures acting on the pipe and found that with an increase in the thickness of the EPS Geofoam, a rapid drop in the pressures acting on the crown was observed up to a certain thickness, and then further increase in EPS Geofoam thickness did not yield any additional positive impact. Placido and Portelinha (2019) conducted physical and numerical model experiments to analyze the effect of geocomposites on underlying pipes and investigated their utilization instead of EPS Geofoam. According to their results, geocomposites perform as well as EPS Geofoam in terms of reducing the pressures acting on the pipe. Hegde and Sitharam (2015) investigated the effect of geocell, geogrid, and a combination of the two reinforcement materials on the pressures acting on the pipe.

*Corresponding author, Assistant Professor
E-mail: selcuk.bildik@nisantasi.edu.tr
[a]Ph.D. Student
E-mail: candasoner3@gatech.edu
[b]Professor
E-mail: david.frost@ce.gatech.edu

ISSN: 2005-307X (Print), 2092-6219 (Online)

According to their results, when the combination of the reinforcements was used, 50% improvement was obtained on the vertical pressure acting on the pipe. Fattah *et al.* (2018) conducted physical and numerical model experiments to determine the effect of geocell reinforcement on the settlement and pressures acting on the pipe. A vertical stress reduction of 41% was obtained after the implementation of geocell reinforcement.

Geotextile reinforcements can also be used in many applications in geotechnics. There are considered to be five nominal different functions of geotextiles. They are used to enhance the efficiency of the system, serving functions including separation, filtration, drainage, protection, and reinforcement. Among them, reinforcement is one of the more important features that geotextiles have. In the literature, it has been shown using both experimental (Kou *et al.* 2018) and numerical (Aria *et al*. 2017) studies that geotextile reinforcements are effective to reduce the effect of the applied loads for some geotechnical structures.

There have been limited studies performed on the effect of geotextile reinforcement on soil-pipe interaction. Kou *et al.* (2018) investigated the effect of the width of the geotextile reinforcement on the buried pipe systems. Four different geotextile widths of 1D, 2D, 3D, and 4D were compared, where D is the diameter of the pipe. They found that an increase in the width of the geotextile leads to a decrease in the pressures acting on the pipe footing and conduit deflection. Kou and Shukla (2021) also investigated the effect of geotextile reinforcement on soil-pipe interaction with numerical analysis using PLAXIS 3D under cyclic loading. According to the results, they verified that pressures acting on the top of the pipe decreases with the geotextile reinforcement. Furthermore, Aria *et al.* (2019) numerically investigated the effect of wrap-around ends of the geotextile on the bearing capacity of the foundation soil and observed a 120% increase in the bearing capacity, which was only 45% with the horizontal layout of the geotextile.

However, in the literature, the effect of tensile stiffness of the geotextile and relative stiffness of the soil with respect to pipe stiffness on the deformation characteristics of the buried pipe was not investigated in detail. Besides, the optimum number and location of geotextile layers with buried pipe systems is unknown. Aria *et al*. (2017) conducted numerical experiments using PLAXIS 2D to understand the optimum location of the geosynthetic reinforcement; however, no simulations were performed in which pipe is installed in the soil. In this work, a numerical model was created with PLAXIS 3D, and parametric studies were conducted by altering the stiffness of the soil, in-plane stiffness of the geotextile reinforcement, elasticity modulus of the buried pipe, footing width, geotextile width, and location of the buried pipe and geotextile reinforcements.

2. Numerical modelling

The finite element analysis software, PLAXIS 3D was used in numerical calculations. PLAXIS 3D is used for modelling geotechnical engineering applications using the finite element method. In total, the model consisted of five different elements; backfill soil, footing, geotextile, pipe, and interfaces. Backfill soil and interface elements were modelled using 10-node tetrahedral elements, while modelling of the footing and pipe was performed by plate elements, which consist of a 6-node triangular element. Likewise, the geotextile was modelled using a geogrid element, which is also a 6-node element. The geogrid element is a tension element, which cannot show any resistance to compressive loads and hence is suitable for modelling geotextiles.

A hardening soil model was implemented in the simulations. This is a hyperbolic soil model which makes use of three different elastic moduli values to better estimate the soil behavior. In this work, since the effect of the parameters that can affect the soil-pipe-geosynthetic behavior varies, composite analyses were performed where in-plane stiffness of the geotextile, modulus of the pipe, and soil stiffness were changed parametrically. A total of 4 different geotextile stiffness (EA), 4 different pipe elasticity (E_{pipe}), and 3 different soil secant stiffness (E_{sec}) values were

Table 1 Numerical properties of soil, pipe, and geotextile

Material	Parameters	Value
Sand	Material Model	Hardening Soil
	Secant Modulus, E_{50} (MPa)	20, 40, 60
	Cohesion, c (kPa)	1
	Friction angle, Φ (°)	37, 41, 45
	Dilatancy angle, Ψ (°)	7, 11, 15
	R_{inter}	0.9
	Dry Unit weight, γ (kN/m^3)	17
Pipe	Young's Modulus, E (MPa)	1000 – 4000
	Poisson ratio, ν	0.38
Geotextile	In-plane Stiffness, EA (kN/m)	100 – 2000

Table 2 Analyses plan

Series	Constant Parameters	Variable Parameters
I	E_{sec} = 60 MPa, EA = 1000 kN/m, B = D, B_g = 4D, H = D/2, L = D/2	E_{pipe} = 1000-4000 MPa
II	E_{pipe} = 3000 MPa, EA = 1000 kN/m, B = D, B_g = 4D, H = D/2, L = D/2	E_{sec} = 20, 40, 60 MPa
III	E_{sec} = 60 MPa, E_{pipe} = 3000 MPa, B = D, B_g = 4D, H = D/2, L = D/2	EA = 100, 500, 1000, 2000 kN/m
IV	E_{sec} = 60MPa, E_{pipe} = 3000 MPa, EA = 1000 kN/m, B_g = 4D, H = D/2, L = D/2	B = 0.5D, D, 1.5D, 2D
V	E_{sec} = 60 MPa, E_{pipe} = 3000 MPa, EA = 1000 kN/m, B = D, H = D/2, L = D/2	B_g = D, 2D, 3D, 4D
VI	E_{sec} = 60 MPa, E_{pipe} = 3000 MPa, EA = 1000 kN/m, B = D, B_g = 4D	H = 0.25D, 0.5D, 0.75D, D L = 0.25D, 0.5D, 0.75D, D

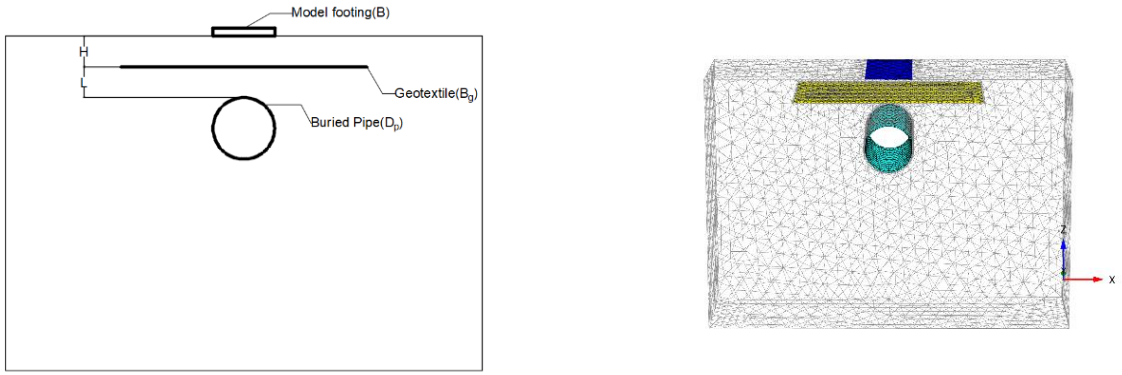

(a) (b)

Fig. 1 Illustration of (a) Schematic of the baseline case and (b) Illustration of the finite element model

compared. Geotextile stiffness values were varied from 100 kN/m to 2000 kN/m. This range was selected because, although in most of the practical works, this value is estimated to be in the range of 100-200 kN/m (Kou and Shukla 2021, Aria *et al*. 2019) nevertheless in some research studies, this range was greater (100 to 1000 kN/m (Wulandari and Tjandra 2015) or 2000 kN/m (Pires and Palmeria 2021)). To reflect a more comprehensive numerical study, the wider range of geotextile reinforcement stiffness values were used. In addition, 4 different pipe moduli values were used (1000, 2000, 3000, and 4000 MPa). Three different soil secant stiffness values were used to represent different soil states (20 MPa for loose, 40 MPa for medium dense, and 60 MPa for dense states). Additionally, the effect of location of the geotextile reinforcement with respect to pipe was investigated at different distances between geotextile and pipe at varying locations. These relative locations are shown in Fig. 1(a), where H is the distance from the footing to the geotextile, and L is the distance from the geotextile to the crown of the pipe. Lastly, the effect of foundation width (B), and geotextile width (B_g) on pipe-geotextile-footing mechanism numerically investigated. To do that, footings with different widths, 0.5D, D, 1.5D. and 2D, and geotextile with different widths, D, 2D, 3D, and 4D were tested, where D is the pipe diameter. Numerical properties of soil, pipe and geotextile can be found in Table 1. In the parametric study, a baseline case was selected (EA = 1000 kN/m, E_{pipe} = 3000 MPa, E_{sec} = 60 MPa, H = D/2, L = D/2, B = D, and B_g = 4D) and comparisons were made with the baseline case. The testing program is summarized in Table 2.

The model boundaries were set according to a sensitivity analysis. In the literature, Kou and Shukla (2021) stated that the distance to the boundaries should be higher than seven times the pipe diameter. Test model geometries were assigned as 124 x 40 x 87 cm. The thickness of the model footing was assigned as 2 cm. Static loading was applied to the footing with a surface pressure of 150 kPa.

Interactions between soil-pipe and soil-geotextile were defined by interface elements. In PLAXIS 3D, an interface reduction factor, R_{inter}, is defined to simulate the interface behavior. In most of the works related to this area (Kou and Shukla 2021, Aria *et al*. 2019) R_{inter} value was given as 0.7.

In this work, first, the effect of R_{inter} on the bending moments on the pipe and pipe deflection was investigated and no significant difference was observed between R_{inter} = 0.7 and 0.9. R_{inter} value was thus selected as 0.9 in this work. System components (footing, geotextile, pipe, interfaces) are shown in Fig. 1(b).

3. Results and discussion

In this study, the aim was to determine the effect of the soil stiffness, in-plane stiffness of the geotextile reinforcement, flexural stiffness of the pipe, geotextile and foundation width, and location of geotextile layers and buried pipe on the effectiveness of the geosynthetic reinforcement. The effects were investigated from two perspectives, the deflection of the pipe, and the bending moment in the pipe. To consider the improvement in deflection of the pipe, a ratio defined as the deflection reduction factor (DRF) as shown in Eq. (1) was calculated

$$DRF = \frac{Deflection\ of\ the\ pipe\ with\ reinforcement}{Deflection\ of\ the\ pipe\ without\ reinfocement} \quad (1)$$

Likewise, to consider the reduction in the bending moment of the pipe, another ratio defined as the bending moment reduction factor (BMRF) as shown in Eq. (2) was calculated

$$BMRF = \frac{Bending\ moment\ of\ the\ pipe\ with\ reinforcement}{Bending\ moment\ of\ the\ pipe\ without\ reinfocement} \quad (2)$$

In the experiments, DRF and BMRF values were determined under applied surface loads of 150 kPa for the different cases.

3.1 The effect of soil stiffness on the efficiency of geotextile reinforcement

In this section, the effect of soil stiffness on the geotextile efficiency is discussed. The parameters other than the soil stiffness were kept the same as the baseline case (H = 8 cm, L= 8 cm, E_{sec} = 60 MPa, E_{pipe} = 3000 MPa, $EA_{geotextile}$ = 1000 kN/m, B_g= 4D). The vertical cross sections of total displacements taken from the center of the

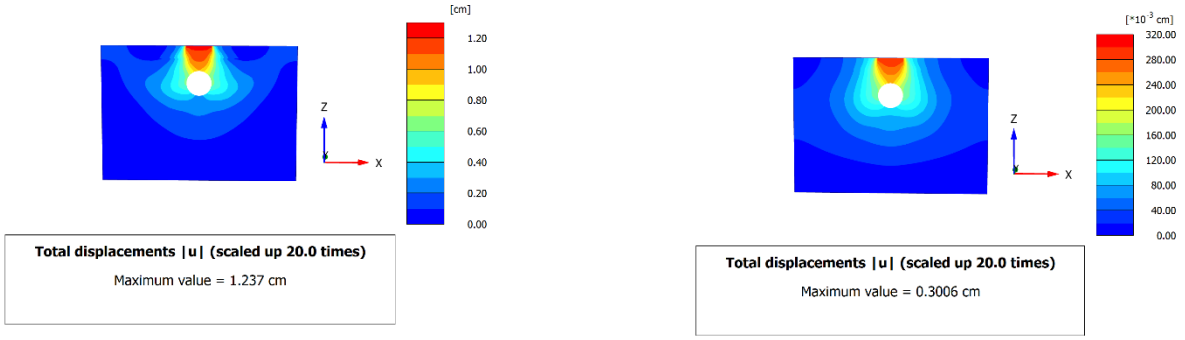

(a) (b)

Fig. 2 Vertical cross section of the soil deformation field for (a) E_{sec}= 20 MPa and (b) E_{sec}= 60 MPa

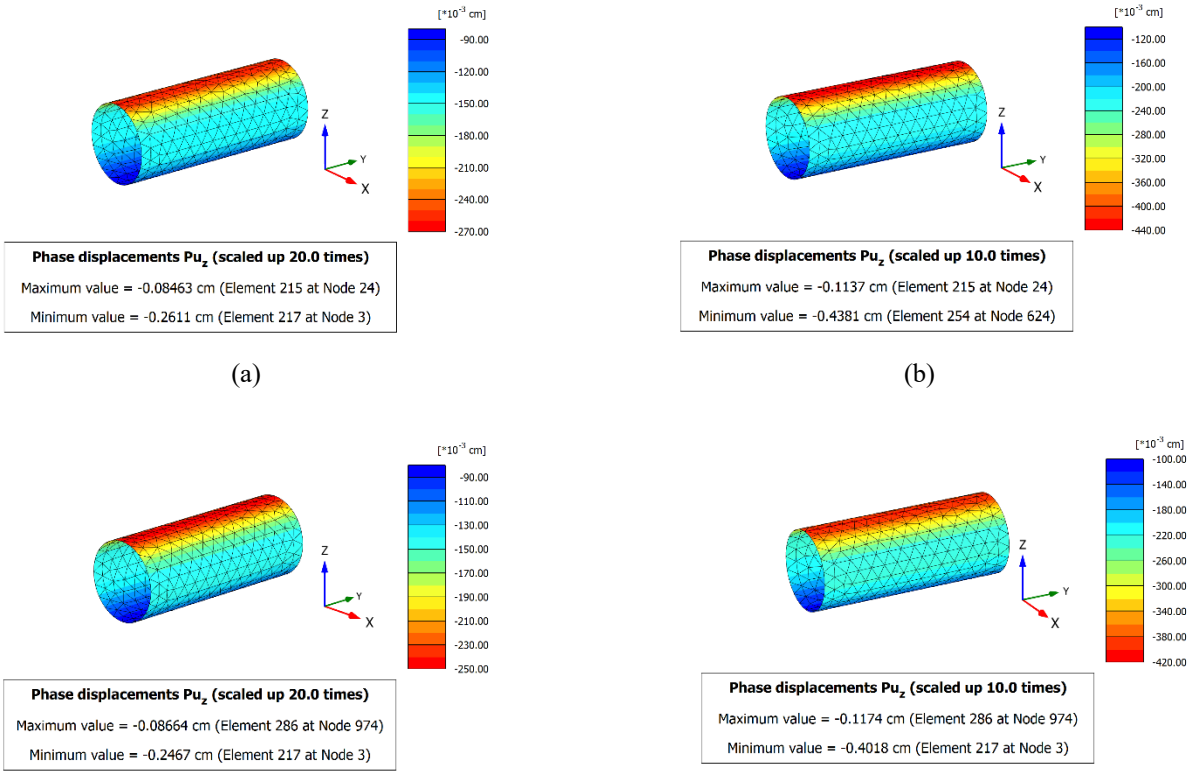

(a) (b)

(c) (d)

Fig. 3 Pipe displacement for (a) Soil E_{sec}= 60 MPa without geotextile, (b) Soil E_{sec}= 40 MPa without geotextile, (c) Soil E_{sec}= 60 MPa with geotextile, and (d) Soil E_{sec}= 40 MPa with geotextile

model box are illustrated in Fig. 2 for E_{sec} = 20 MPa and E_{sec} = 60 MPa, respectively. In Fig. 2, in the less stiff soil, a passive soil zone was observed, while with the increase in the friction angle, a larger distance was required for the passive zone to be developed. This passive zone in the stiffer soil reached the boundaries. In Fig. 3, the change in surficial displacement of the pipe is illustrated for baseline case (E_{sec} = 60 MPa) and E_{sec} = 40 MPa. Although the deformation pattern was not significantly changed, the BMRF and DRF values changed. As summarized in Fig. 4, with the increase in the soil stiffness, there was a decrease in the reduction factors between E_{sec} = 20 MPa and E_{sec} = 40 MPa. Conversely, an increase in the stiffness from 40 MPa to 60 MPa led to an increase in the reduction factors.

The optimum geotextile efficiency is a function of the pipe and soil stiffness, so based on the baseline case pipe stiffness parameters, optimum soil stiffness reached at about 40 MPa. However, the coupled mechanism between the pipe and soil stiffness can change the geotextile efficiency.

3.2 Effect of in-plane stiffness of the geotextile on DRF and BMRF

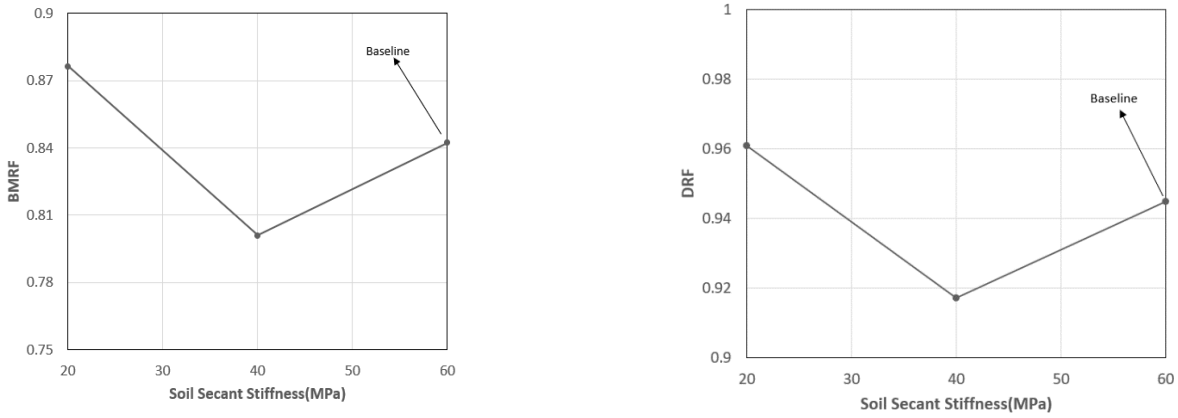

(a) (b)

Fig. 4 Change in (a) Bending moment reduction factor (BMRF) and (b) Deflection reduction factor (DRF) for different soil secant stiffnesses

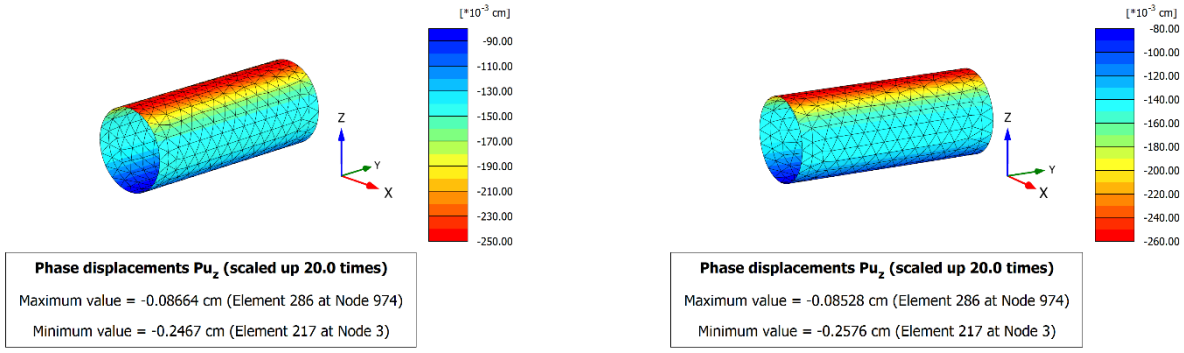

(a) (b)

Fig. 5 Pipe displacement for in-plane geotextile stiffness (a) EA=1000 kN/m (b) EA=100 kN/m

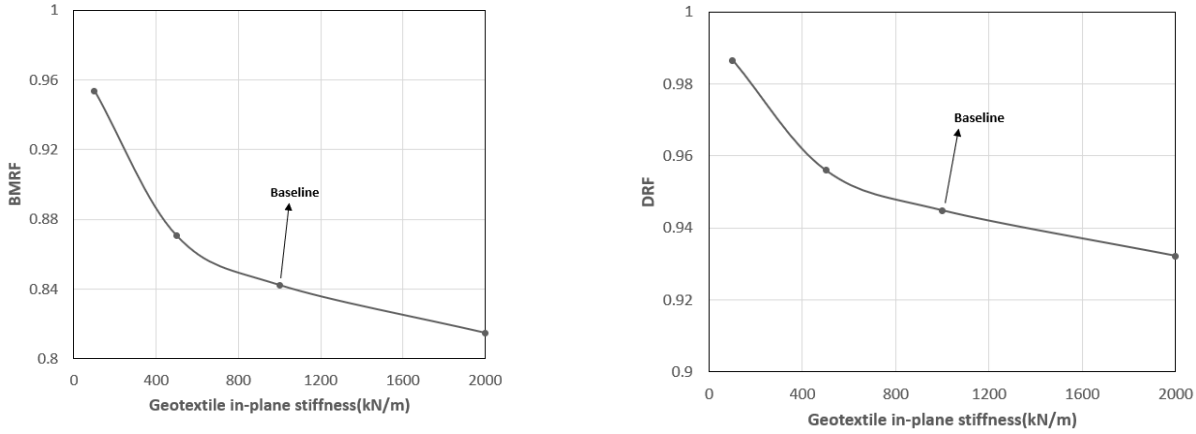

(a) (b)

Fig. 6 Change in (a) Bending moment reduction factor (BMRF) and (b) Deflection reduction factor (DRF) for different geotextile in-plane stiffnesses

The effect of the geotextile in-plane stiffness on DRF and BMRF is discussed in this section. By changing the geotextile stiffness between 100, 500, 1000, and 2000 kN/m, the effect of in-plane stiffness of the geotextile was examined. In the baseline case, the in-plane geotextile stiffness was 1000 kN/m. The displacement profile of the pipe under the application of the load for EA = 1000 kN/m and EA = 100 kN/m is shown in Fig. 5. The results are

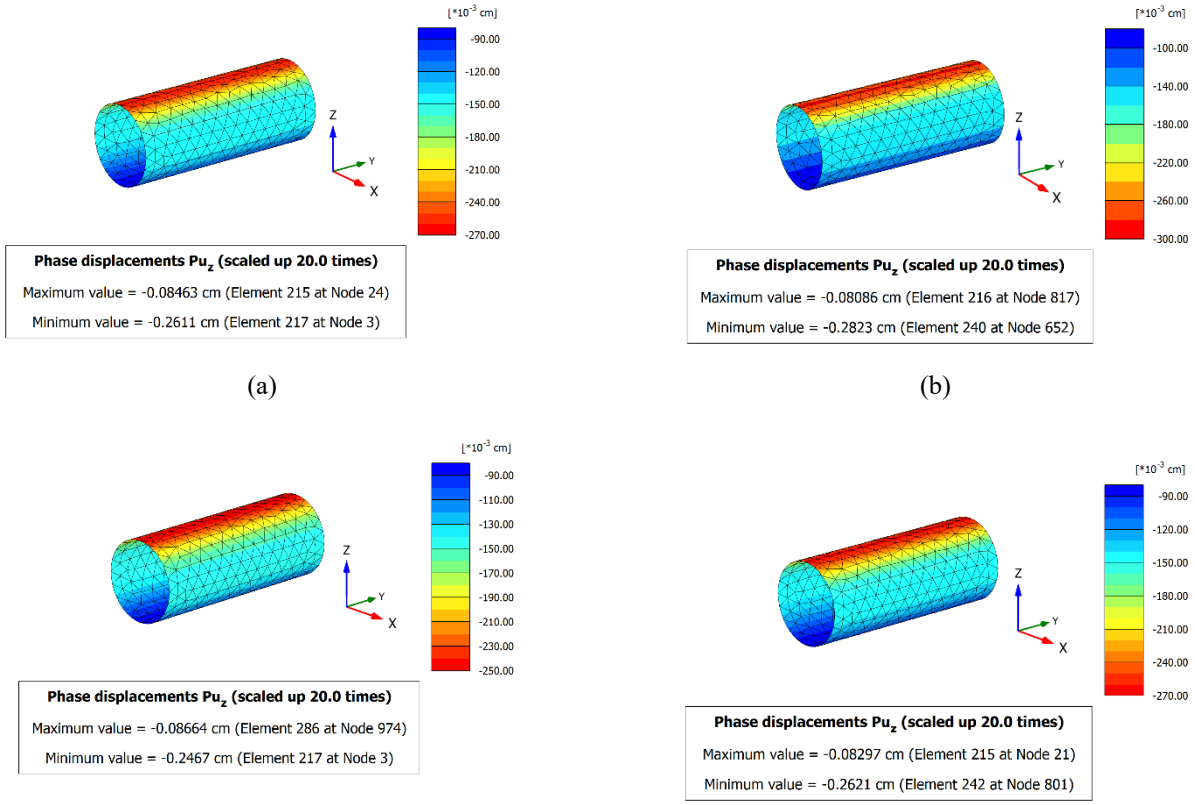

Fig. 7 Pipe displacement for (a) E_{pipe}= 3000 MPa without geotextile, (b) E_{pipe}= 1000 MPa without geotextile, (c) E_{pipe}= 3000 MPa with geotextile, and (d) E_{pipe}= 1000 MPa with geotextile

illustrated in Fig. 6 for DRF and BMRF. As seen in Fig. 6, with the increase in the strength of the geotextile from 100 kN/m to 2000 kN/m, a decrease in both DRF and BMRF values was observed. With the increase in the in-plane stiffness of the geotextile, the severity of the decrease also decreased i.e., the difference between 1000 and 2000 kN/m was lower than the difference between 100 and 500 kN/m.

The reasoning behind those changes is explained as follows. When the geotextile reinforcement was added to a system, load was distributed to the system differently. Some of the load was dissipated with the tensile strain in the geotextile layer; therefore, under the geotextile layer, the load increase was lower. This caused a lower displacement, and hence a lower bending moment. With the increase in the geotextile stiffness, higher energy was dissipated in the geotextile layer; therefore, the induced load under the geotextile layer was lower compared to that with a geotextile having lower stiffness.

3.3 Effect of pipe stiffness on DRF and BMRF

Numerical studies were performed with different values of pipe elastic modulus while keeping every other parameter the same with the baseline case. Displacement fields for E_{pipe} = 1000 MPa and 3000 MPa with and without geotextiles are illustrated in Fig. 7. The cases without geotextiles are included to provide the readers with the actual DRF. The results of the change in the DRF and BMRF for different pipe stiffness values are summarized in Fig. 8. It can be seen that an increase in the pipe stiffness led to an increase in the reduction factors, which means that the effect of the geotextile diminished with an increase in the pipe stiffness. Therefore, a suitable pipe/geotextile stiffness ratio should be selected to optimize the improvement. Similarly, an increase in pipe stiffness led to an increase in DRF, as illustrated in Fig. 8.

3.4 Effect of geotextile width on DRF and BMRF

Additionally, some numerical simulations were conducted with different geotextile widths. Four different geotextile width values were analyzed. The comparison of pipe displacement when geotextile width is 4D (baseline) and D is shown in Fig. 9. The results of the change in the DRF and BMRF for different geotextile in-plane stiffness values are illustrated in Fig. 10. The increase in geotextile width yielded a decrease in the reduction factors between D and 2D but did not yield significant additional reductions for greater widths. In these analyses, this optimum geotextile width/pipe diameter ratio was reached at about 2D.

3.5 Effect of footing width on DRF and BMRF

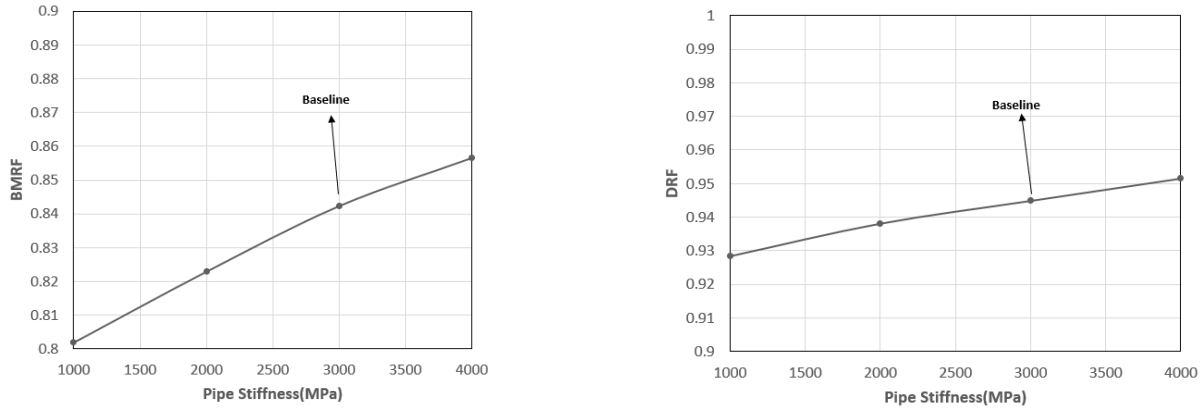

(a) (b)

Fig. 8 Change in (a) Bending moment reduction factor (BMRF) and (b) Deflection reduction factor (DRF) for different pipe stiffnesses

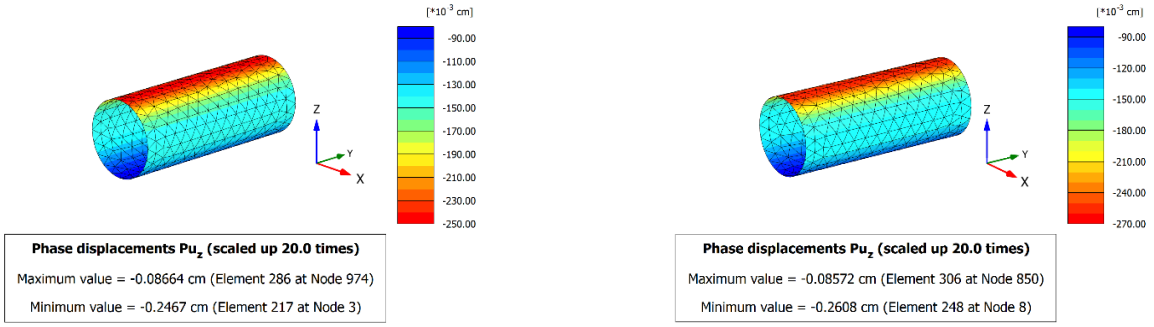

(a) (b)

Fig. 9 Pipe displacement for geotextile width (a) 4D and (b) D

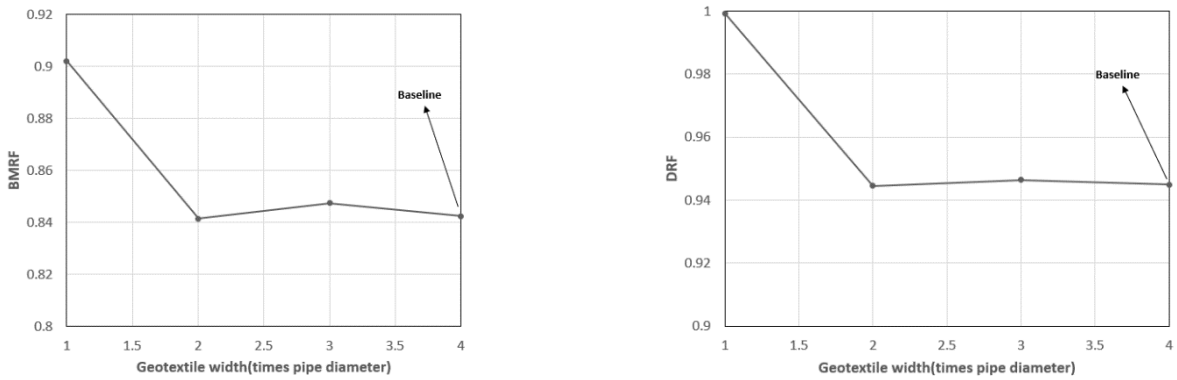

(a) (b)

Fig. 10 Change in (a) Bending moment reduction factor (BMRF) and (b) Deflection reduction factor (DRF) for different geotextile widths

The effect of surface footing width on the geotextile efficiency in protecting the buried utility is also investigated with four different footing widths, which are 0.5D, D, 1.5D, and 2D. The vertical cross sections of total displacements for the cases where footing width is D and 2D are shown in Fig. 11. As illustrated in Fig. 11, while the concentration of the displacement occurred on the crown of the pipe when foundation width was equal to D, it spread to a wider region when the footing width was increased to 2D. The displacement fields for pipes for the cases with and without geotextile for footing width D (baseline) and 2D are shown in Fig. 12. A summary of the results obtained for all footing widths is illustrated in Fig. 13. When the footing width was equal to the pipe diameter, the most efficient results were observed in terms of BMRF and DRF.

3.6 Effect of location of the pipe and geotextile on DRF and BMRF

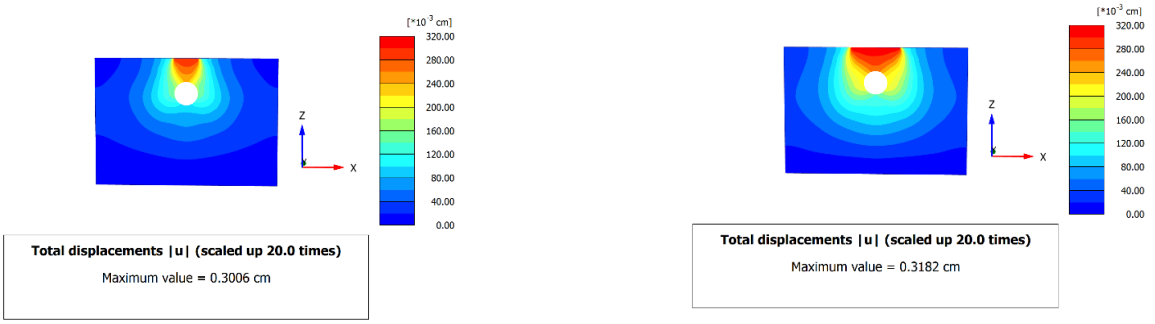

(a) (b)

Fig. 11 Vertical cross section of the soil deformation field for foundation width (a) D and (b) 2D

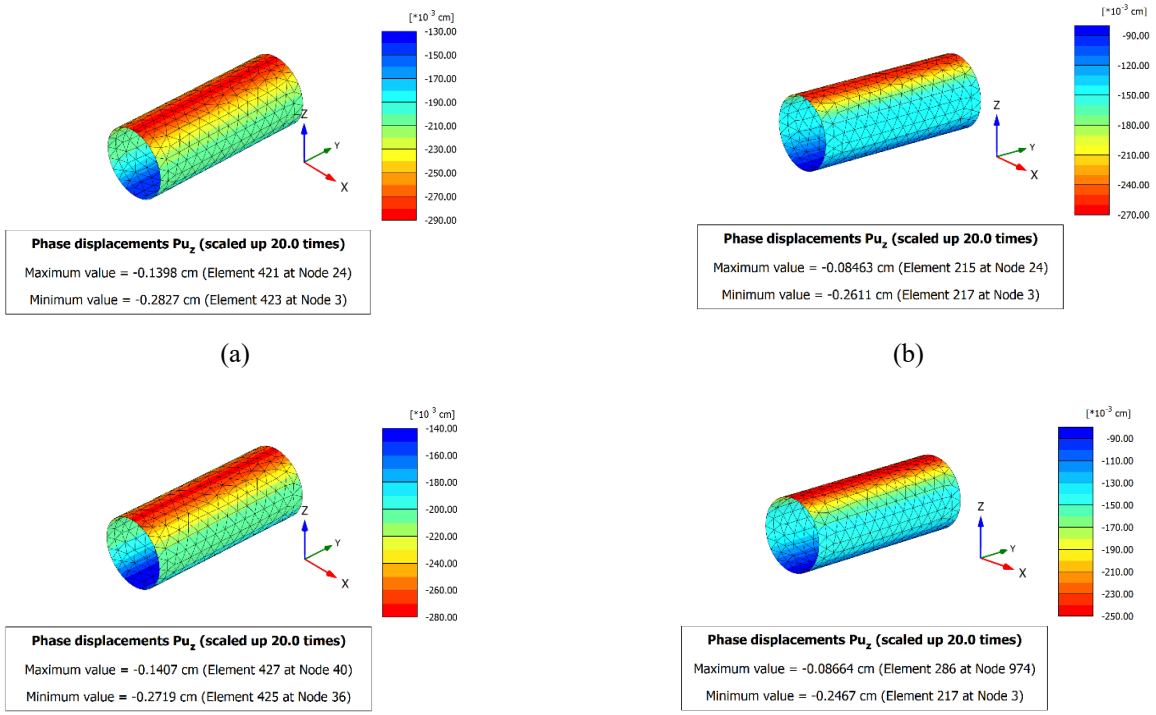

(a) (b)

(c) (d)

Fig. 12 Pipe displacement for (a) foundation width 2D without geotextile, (b) foundation width D without geotextile, (c) foundation width 2D with geotextile, and (d) foundation width D with geotextile

Additional analyses were conducted in order to better understand and estimate the effect of geotextile reinforcement for different pipe and geotextile locations. To do that, the geotextile was fixed at one depth, and the pipe was shifted from an upper closer elevation to greater depths systematically. This process was repeated for several different initial geotextile depths, and results are summarized in Fig. 14. With the increase in the distance between geotextile and pipe, regardless of the initial geotextile burial depth, there was an increase in the BMRF and DRF, meaning that the efficiency of the geotextile was diminished. When the primary reason for the geotextile is to protect the pipe, according to the results, the closer it is to the pipe, the better efficiency is obtained.

4. Numerical validation

In order to validate and extend the results of this numerical study, additional numerical validation was performed using the experimental results presented in Bildik and Laman (2020) paper. In their work, geogrid reinforcement was used to: 1) increase the bearing capacity of a foundation over a pipe-soil system, 2) reduce the footing settlement, and 3) reduce the hoop stresses on the pipe. Numerical validation was performed using the load-settlement data obtained from the Bildik and Laman (2020) experimental work. The experimental and numerical results are illustrated in Fig. 15.

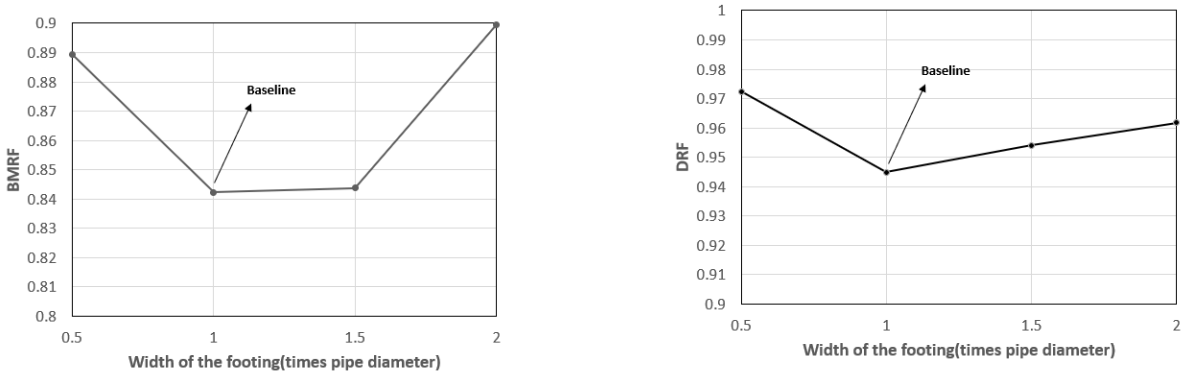

(a) (b)

Fig.13 Change in (a) Bending moment reduction factor (BMRF) and (b) Deflection reduction factor (DRF) for different footing widths

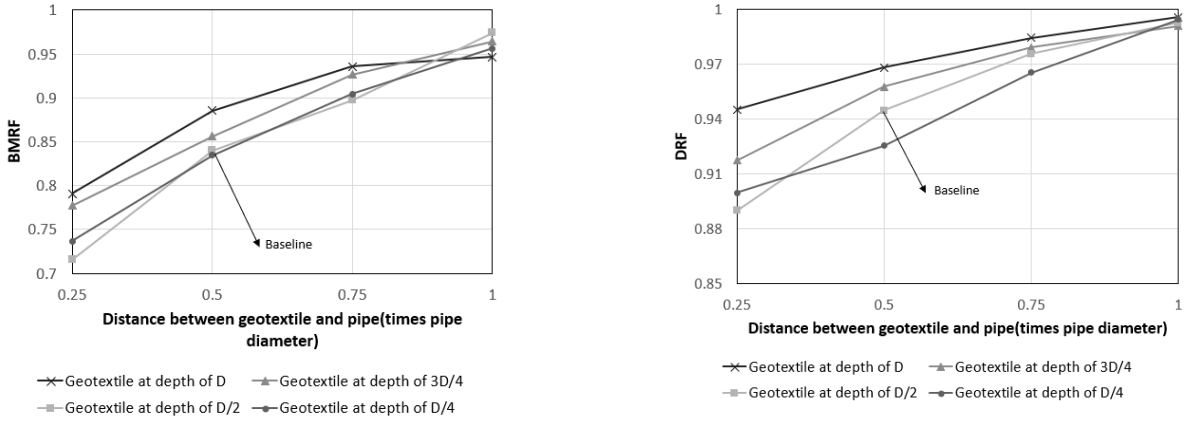

(a) (b)

Fig.14 Change in (a) Bending moment reduction factor (BMRF) and (b) Deflection reduction factor (DRF) for different pipe and geotextile locations

In numerical validation, to calibrate the model and identify appropriate soil properties, an unreinforced numerical case was created by altering the parameters systematically to match the unreinforced experimental case. Upon completion of this, geotextile reinforcement was added to the system with different burial depths, and a comparison was made with the corresponding experimental reinforced case. The H/B ratio in Fig. 15 represents the ratio of the burial depth of the geosynthetic to the footing width. Although a very similar load-settlement curve was captured in the unreinforced case for numerical and experimental models, the numerical model slightly under-predicted the applied pressure at the same footing settlement to footing width ratio. This under-prediction is hypothesized to be due to the particle interlocking effect of the geogrids, which isnot seen in geotextiles. In that, the focus of the present study is to evaluate the relative BMRF and DRF values, this variation in the calibration for reinforced cases is considered acceptable.

5. Conclusions

- In this study, numerical simulations were performed in order to understand the effect of in-plane stiffness of the geotextile reinforcement, the elastic modulus of the pipe, soil stiffness, footing and geotextile width, and the location of the geotextile layers on the bending moments in the pipe and deflections of the pipe. Results are summarized as bending moment reduction factors (BMRF) and deflection reduction factors (DRF). The main findings of this study are summarized below: In the analyses, for the investigated region, optimum soil stiffness to maximize the geotextile efficiency was identified. This optimum soil stiffness is a function of the other investigated parameters; therefore, additional rigorous research should be performed to understand which soil stiffness might maximize the effects of a geotextile reinforcement for a specific soil-geotextile-pipe combination.
- There is a relationship between in-plane stiffness of the geotextile and BMRF and DRF. It is observed that with the increase in the geotextile reinforcement, both reduction factors tend to decrease. The amount of decrease is more significant when the in-plane stiffness is lower, and the positive effect of the additional stiffness tends to deteriorate with the increase in the stiffness values. Up to 19% reduction is observed in BMRF, while the corresponding value is 7% for DRF.

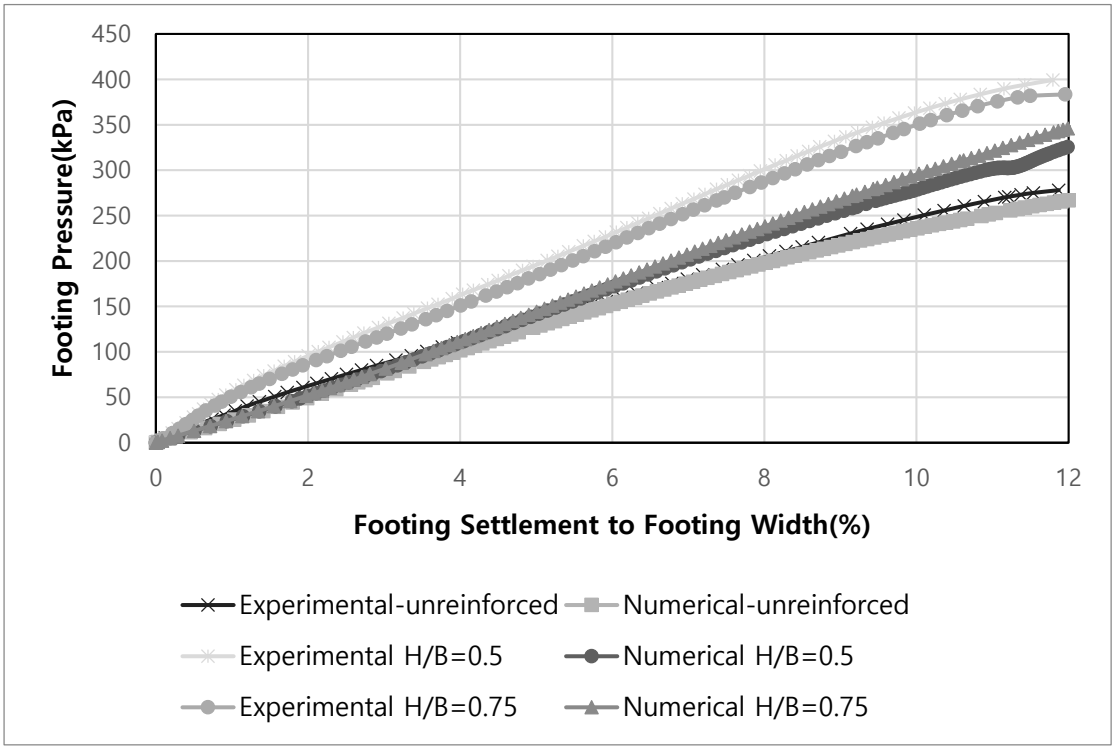

Fig.15 Load-settlement curves for reinforced and unreinforced cases for numerical and experimental (Bildik and Laman (2020)) studies

- The results show that pipe stiffness is also a determining factor in the effect of the geotextile reinforcement. With the increase in the pipe stiffness, DRF and BMRF increases, which means that for the given soil and geotextile properties, geotextile reinforcement becomes less effective.
- It is determined that the geotextile width should be in the range of D to 1.5 D to benefit from the geotextile layer in the most efficient way.
- Similarly, the effect of geotextile layer is observed as more prominent when the footing width is equal to the pipe diameter.
- Changing the position of the geotextile reinforcement layers with respect to pipe also caused some differences in BMRF and DRF values. In general, regardless of the pipe burial depth, when the geotextile reinforcement is closer to the pipe, reinforcement becomes more effective in reducing BMRF and DRF.
- In general, when the various conditions and effects are compared, it is found that geotextile reinforcement is more efficient to reduce the bending moments acting on the pipe compared to the deflection of the pipe.

Acknowledgments

The participation of the first and third authors in the study reported in this manuscript was supported in part by the US National Science Foundation through the Engineering Research Center on Bio-mediated and Bio-inspired Geotechnics (CBBG). The NSF support through PTE Federal Award No. EEC-1449501 is gratefully acknowledged. The opinions in the manuscript are those of the authors and not the sponsor.

References

Aria, S., Shukla, S.K. and Mohyeddin, A. (2017), "Optimum burial depth of geosynthetic reinforcement within sand bed on numerical investigation", *Int. J. Geotech. Eng.*, **14**(1), 71-79. https://doi.org/10.1080/19386362.2017.1404202.

Aria, S., Shukla, S.J. and Mohyeddin, A. (2019), "Numerical investigation of wraparound geotextile reinforcement technique for strengthening foundation soil", *Int. J. Geomech.*, **19**(4). https://doi.org/10.1061/(ASCE)GM.1943-5622.0001361.

Beju, Y.Z. and Mandal, J.N. (2017), "Combined use of Jute geotextile-EPS geofoam to protect flexible buried pipes: experimental and numerical studies", *Int. J. Geosynth. Ground Eng.*, **3**, Article Number: 32. https://doi.org/10.1007/s40891-017-0107-5.

Bildik, S. and Laman, M. (2015), "Experimental investigation of the effects of pipe location on the bearing capacity", *Geomech. Eng.*, **8**(2), 221-235. https://doi.org/10.12989/gae.2015.8.2.221.

Bildik, S. and Laman, M. (2019), "Experimental Investigation of Soil-Structure-Pipe Interaction", *KSCE J. Civil Eng.*, **23**, 3753-3763. https://doi.org/10.1007/s12205-019-0134-y.

Bildik, S. and Laman, M. (2020), "Effect of geogrid reinforcement on soil-structure-pipe interaction in terms of bearing capacity, settlement and stress distribution", *Geotext. Geomembranes*, **48**(6), 844-853. https://doi.org/10.1016/j.geotexmem.2020.07.004.

Elshesheny, A., Mohamed, M., Nagy, N.M. and Sheehan, T. (2020), "Numerical behavior of buried flexible pipes in geogrid-reinforced soil under cyclic loading", *Comput. Geotech.*, **122**, 103493. https://doi.org/10.1016/j.compgeo.2020.103493.

Fattah, M.Y., Hassan, W.H. and Rasheed, S.E. (2018), "Behavior of flexible buried pipes under geocell reinforced subbase subjected to cyclic loading", *Int. J. Geotech. Earthq. Eng.*, **9**(1), 22-41. https://doi.org/10.4018/IJGEE.2018010102.

Hegde, A.M. and Sitharam, T.G. (2015), "Experimental and numerical studies on protection of buried pipelines and underground utilities using geocell", *Geotext. Geomembranes*, **45**(3), 372-381. https://doi.org/10.1016/j.geotexmem.2015.04.010.

Kou, Y., Shukla, S.K. and Mohyeddin, A. (2018), "Experimental investigation for pressure distribution on flexible conduit covered with sandy soil reinforced with geotextile reinforcement of varying widths", *Tunn. Undergr. Sp. Tech.*, **80**, 151-163. https://doi.org/10.1016/j.tust.2018.06.012.

Kou, Y. and Shukla, S.K. (2019), "Analytical Investigation of Load Over Pipe Covered with Geosynthetic-Reinforced Sandy Soil", *Int. J. Geosynth. Ground Eng.*, **5**(1), 1-8. https://doi.org/10.1017/s40891-019-0156-z.

Kou, Y. and Shukla, S.K. (2021), "Numerical modelling of unreinforced and geosynthetic reinforced sandy soil cover over large diameter HDPE and PVC pipes", *Geotech. Geol. Eng.*, **39**, 1689-1699. https://doi.org/10.1007/s10706-020-01548-3.

Ma, Q., Ku, Z. and Xiao, H. (2019), "Model tests of earth pressure on buried rigid pipes and flexible pipes underneath expanded polystyrene (EPS)", *Adv. Civil Eng.*, **2019**, Article ID 9156129. https://doi.org/10.1155/2019/9156129.

Pires, A.C.G. and Palmeira, E.M. (2017), "Geosynthetic protection for buried pipes subjected to surface surcharge loads", *Int. J. Geosynth. Ground Eng.*, **3**, Article Number: 30. https://doi.org/10.1007/s40891-017-0109-3.

Pires, A.C.G. and Palmeira, E.M. (2021), "The influence of geosynthetic reinforcement on the mechanical behavior of soil-pipe systems", *Geotext. Geomembranes*, **49**(5), 1117-1128. https://doi.org/10.1016/j.geotexmem.2021.03.006.

Placido, R. and Portelinha, F.H.M. (2019), "Evaluation of geocomposite compressible layers as induced trench method applied to shallow buried pipelines", *Geotext. Geomembranes*, **47**(5), 662-670. https://doi.org/10.1016/j.geotexmem.2019.103471.

Wulandari, P.S. and Tjandra, D. (2015), "Analysis of geotextile reinforced road embankment using PLAXIS 2D", *Procedia Eng.*, **125**, 358-362. https://doi.org/10.1016/j.proeng.2015.11.075.

IC